Article ID: 1003－6326(2005)01－0007－07

Microstructure and mechanical properties of magnesium alloy prepared by lost foam casting①

TIAN Xue-feng(田学锋), FAN Zi-tian(樊自田), HUANG Nai-yu(黄乃瑜),
WU He-bao(吴和保), DONG Xuan-pu(董选普)
(State Key Laboratory of Plastic Forming and Die & Mould Technology,
College of Materials Science and Engineering, Huazhong University of Science and Technology,
Wuhan 430074, China)

Abstract: The microstructure and mechanical properties of AZ91 alloy prepared by lost foam casting(LFC) and various heat treatments have been investigated. The microstructure of the AZ91 alloy via LFC consists of dominant α-Mg and β-$Mg_{17}Al_{12}$ as well as a new phase $Al_{32}Mn_{25}$ with size of about 5－50 μm, which has not been detected in AZ91 alloy prepared by other casting processes. The tests demonstrate that the as-cast mechanical properties are higher than those of sand gravity casting because of chilling and cushioning effect of foam pattern during the mould filling. The solution kinetics and the aging processes at different temperatures were also investigated by hardness and electrical resistivity measurements. The kinetics of aging are faster at the high temperature due to enhanced diffusion of atoms in the matrix, so the hardness peak at 380 ℃ occurs after 10 h; while at the lower aging temperature (150 ℃), the peak is not reached in the time(24 h) considered.

Key words: magnesium alloy; lost foam casting; mechanical property; microstructure
CLC number: TG146.2 **Document code:** A

1 INTRODUCTION

Magnesium alloys are attractive for applications in the automobile and aerospace industry due to the lower density of magnesium compared with aluminum, improved damping ability, higher resistance to corrosion, and better mechanical properties[1, 2]. The alloy AZ91, based on the Mg-9% Al(mass fraction) system and containing small amounts of zinc, is one of the most widely applied materials of the commercial magnesium alloys. AZ91 alloy workpieces are usually fabricated by various casting processes because of low formability near room temperature. The applicable methods are high-pressure die casting and all kinds of gravity casting such as sand, permanent and semi-permanent mould casting. Other relevant production technologies are squeeze casting, semi-solid casting and rapid solidification[3－7]. The high-pressure die casting dominates among the casting methods used worldwide. However, entrapped gas pores as a result of high fill-up-rate make the casting impossible for heat treatments, and the presence of bands of porosity and segregation in die casting has a significant effect on the mechanical properties[8, 9]. Furthermore, the complicated and expensive production equipment also restricts its application. In order to exploit the benefits of magnesium alloy, it is necessary to develop alternative processing that can effectively produce complex, high-precision casting with good mechanical properties at low expense.

The lost foam casting(LFC) processing or evaporative casting processing is a low-cost technique for manufacturing complicated and near-net-shape castings. In the LFC process molten metal is poured into a foam pattern that has been coated with a refractory material and surrounded with unbounded sand. The pattern evaporates, the molten metal takes the place of the pattern, and the metal solidifies in the shape of the pattern. The LFC process can offer advantages and significant savings over traditional green sand casting by producing castings with lower dimensional tolerances and complex geometries, eliminating or reducing machining and assembly operation, and providing cleaner and quieter working conditions. The LFC of magnesium alloys could emerge as a cost-effective alternative to the high-pressure casting of magnesium workpieces. The LFC of several important alloys including aluminum alloy and cast iron has been studied and applied successively for many years[10－14]. However, the LFC processing of magnesium alloys faces critical challenges due to the high chemical reactivity of magnesium itself and low latent heat compared with aluminum alloys. Up to now, research on LFC of magnesium alloy

① **Foundation item:** Project(50275058) supported by the National Natural Science Foundation of China
Received date: 2004－06－24; **Accepted date:** 2004－11－10
Correspondence: TIAN Xue-feng, PhD; Tel: +86-27-87543876; E-mail: helloonline@etang.com

has concentrated primarily on mold filling behaviors and generation of defects[15, 16]. It is necessary to study the effect of LFC processing and subsequent various heat treatments on microstructures and mechanical properties.

The objective of this paper is to assess the mechanical properties of magnesium alloys prepared by LFC processing, and to correlate these properties with the microstructure, the casting parameters and the various heat treatment conditions.

2 EXPERIMENTAL

The ingots of commercial AZ91 alloy, the composition of which is listed in Table 1, were melted in the laboratory resistance furnace with a steel crucible containing approximately 6 kg of metal and protected by CO_2 + 0.5% SF_6 atmosphere. After attainment of equilibrium at 750 ℃, the melt was degassed for 5 - 10 min using carbon hexachloride tablets. The temperature was reduced stepwise to 740, 710 and 680 ℃. Afterwards, the melts were held for 20 min at each pouring temperature for the deposition of precipitated intermetallics. The temperature fluctuation during holding was typically ±1 ℃. The homogeneous melt was then poured into the downsprue(30 mm × 30 mm × 170 mm) located above the gating system and it vaporized the gating and patterns(135 mm × 20 mm × 20 mm) which were cut from an EPS foam plank using a hot wire cutter and had a nominal density of 0.020 g/cm^3. The molten metal displaced the Styrofoam pattern with precise dimensional accuracy. Gases produced due to the vaporized polystyrene foam pass through the coating layer on the foam pattern and the compacted sand, and through the vents that are located on the flask walls and connected to a container with a constant degree of vacuum (0.04 MPa), produced by a vacuum pump.

Table 1 Chemical compositions of investigated AZ91 alloy(mass fraction, %)

Element	Al	Zn	Mn	Si
Chemical composition	9.207 5	0.628 2	0.291 2	0.044 9

Element	Fe	Cu	Ni	Be	Mg
Chemical composition	0.003 8	0.002 5	0.000 9	0.001 2	Bal.

In this work homogenization heat treatment (T4) for as-cast specimens poured at 710 ℃ was performed at 420 ℃ for 24 h followed by water quench at 15 ℃. The solid-treated alloy was aged artificially(T6) in a series of tests with 4 h interval from 4 h to 24 h at both 380 ℃ and 150 ℃, to produce varying β volume fractions of specimen. Both solution treatment and aging treatment were carried out with a temperature accuracy of ±1 ℃ under a gas shield of SO_2 in the oven.

Optical microscope(OM) and scanning electron microscope(SEM) samples were etched with a solution of 5% nitric acid(volume fraction) + ethyl alcohol. Microanalysis in the alloys studied was conducted using Electron Probe Microanalysis (EPMA). The specimens (1.5 mm × 1.4 mm × 110 mm) suitable for measurements of electrical resistivity in heat treatment were cut from the as-cast samples using an electric spark machine. The values of hardness and electrical resistivity were measured in the different heat treatment conditions using sclerometer and dc four-arm bridge, respectively. Tensile test bars were fabricated to a gauge length of 80 mm and a gauge diameter of 10 mm, and the tensile tests were carried out at a strain rate of 1 mm/min in a materials test machine.

3 RESULTS AND DISCUSSION

3.1 Microstructural observations

The microstructure of the AZ91 magnesium alloy consists of a bimodal distribution of α-Mg grains together with intergranular β-$Mg_{17}Al_{12}$ phase, as reported earlier[17, 18]. Fig. 1(a) shows a typical microstructure and morphology of the AZ91 magnesium alloy via LFC at 710 ℃. The primary rosette-shaped dendrite of the AZ91 alloy is the α-Mg. The size of the grains varies from 320 μm to 41 μm and the average size is measured to be 174 μm. The eutectic structure takes a completely divorced form, in which massive particles of $Mg_{17}Al_{12}$ are surrounded by magnesium solid solution. The amount of discontinuous β($Mg_{17}Al_{12}$) phase in as-cast Mg-9Al-1Zn is 2.88%, which was measured by quantitative metallography. It can be seen that the dominant precipitation morphology is discontinuous. Fig. 1(b) shows the optical microstructure of the AZ91 solution-treated at 420 ℃ for 24 h. The grain size is increased compared to the as-cast state and the precipitate is not yet completely dissolved in the matrix. This means that some content of Mg and Al don't contribute during the aging process at the lower temperature. Artificial aging causes precipitation of the β($Mg_{17}Al_{12}$) phase, as shown in Figs. 1(c) and (d). For the 24 h aging at 380 ℃, the precipitates appear as a continuous pattern at grain boundaries and in the grains. However, for the 24 h aging at 150 ℃, the discontinuous precipitates emerge at grain boundaries and have a massive form. The discontinuous precipitates appear dark due to the low magnification of observation and the presence of β($Mg_{17}Al_{12}$).

EPMA analyses have been performed on the

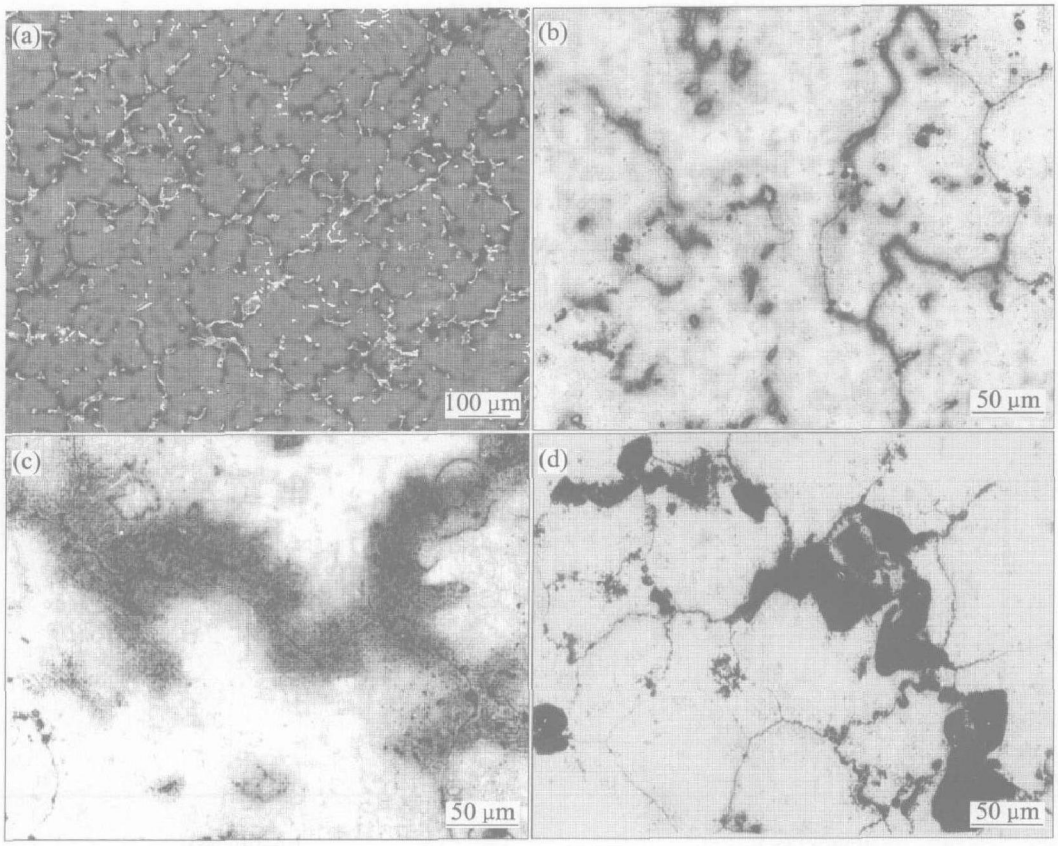

Fig. 1 Scanning electron micrograph(a) of as-cast AZ91 alloy and optical micrographs showing AZ91 alloy in three microstructural states after different heat treatment
(b) —Solution-treated for 24 h at 420 ℃; (c) —Aged for 24 h at 380 ℃; (d) —Aged for 24 h at 150 ℃

as-cast alloy. Fig. 2 shows the electronic energy dispersive spectra of the two precipitate phases and the dominant α-Mg phase in the AZ91 alloys via LFC. The results indicate that another precipitate, not $Mg_{17}Al_{12}$, is rich in Al and Mn with a little amount of Mg. The phases identified in the as-cast samples by EPMA are listed in Table 2. It can be seen that the Mg/Al molar ratio(96.19/3.51) in the matrix is not consistent with the nominal one owing to the formation of the precipitates. For $Mg_{17}Al_{12}$ phase, the Mg/Al molar ratio (63.39/34.58) in the spectrum is higher than the nominal ratio of 17/12, which may be attributed to the Mg matrix. The Al/Mn molar ratio(52.65/41.06) in another phase is lower than that of Al_8Mn_5, which is usually presented in as-cast AZ91 alloy. It is a new phase with size of about 5 ~ 50 μm that has not been reported earlier in the literatures. The phase is written as $Al_{32}Mn_{25}$ in this paper. The amount of Mg may be attributed to the matrix. The generation of the $Al_{32}Mn_{25}$ phase might be associated with special cooling behaviors during the LFC. The formation of a phase depends upon both thermodynamics and kinetic factors. Thermodynamic conditions define a set of possible alloy microstructures with lower free energy than the starting state before phase change. Kinetic behavior determines which of these microstructures actually develops during solidification. More detailed work is being carried out.

Table 2 Analyzed chemical compositions of phases(molar fraction, %)

Phase	Mg	Al	Zn	Mn	Fe	Si
Matrix	96.19	3.51	0.30			
$Mg_{17}Al_{12}$	63.39	34.58	2.03			
$Al_{32}Mn_{25}$	4.70	52.65	0.16	41.06	0.62	0.81

3.2 Solution and ageing curves

Fig. 3 illustrates the hardness curves of the AZ91 alloys via LFC after exposure at 420 ℃. The first point(0 h) of the hardness curve corresponds to the value of the as-cast state and it is always higher than that of the solution-treated samples. The treatment shows a slight decrease of hardness with time. There exist two opposing processes, the solution hardening operated by Mg and Al atoms and the softening action of grain growth, which affect the hardness of the AZ91 alloys during solution treatment. It is probable that the solution hardening cannot compensate for the softening effect and the hardness decreases continuously with time.

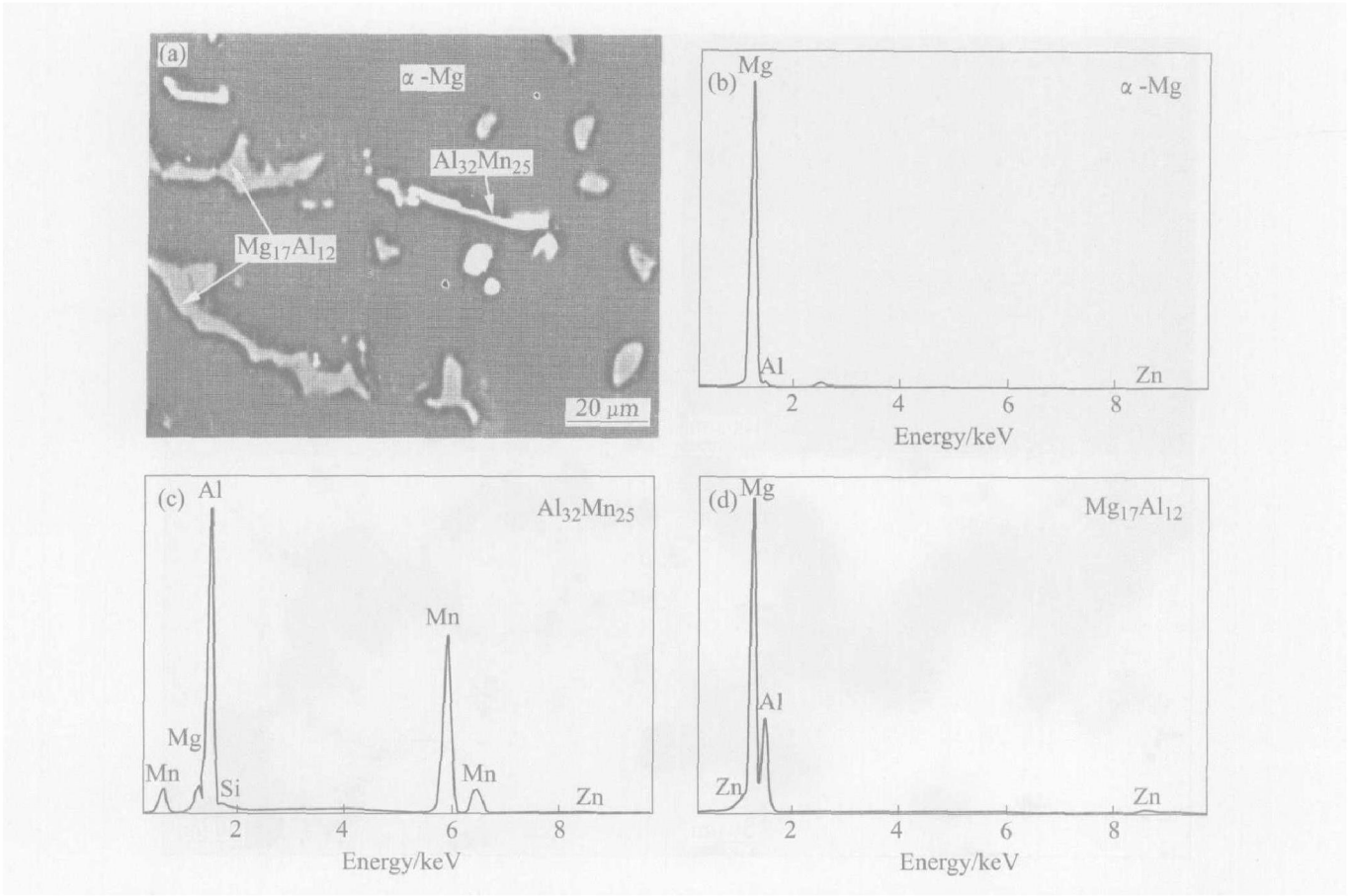

Fig. 2 Typical microstructure(a) and electronic energy dispersive spectra of α-Mg phase and two precipitate phases in AZ91 alloys via LFC

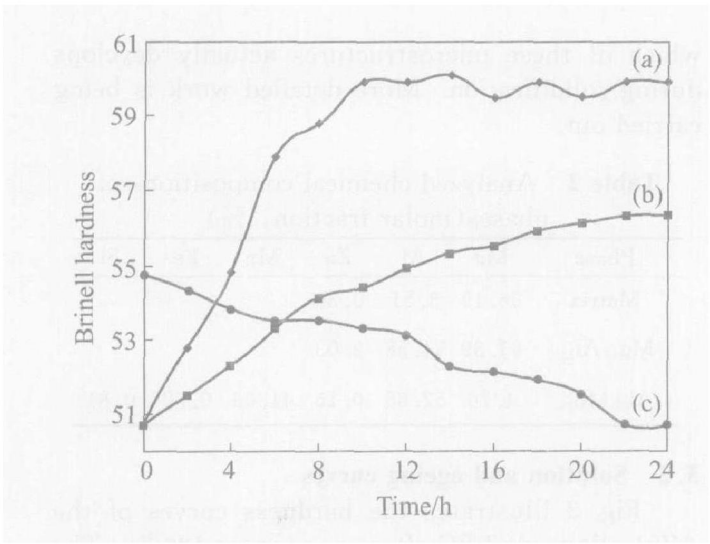

Fig. 3 Hardness curves for AZ91 alloy
(a) —Aged at 380 ℃; (b) —Aged at 150 ℃;
(c) —Solution-treated at 420 ℃

The variation of hardness with ageing time at 150 ℃ and 380 ℃ is also shown in Fig. 3. The shapes of the curves are normal types in all the alloys. The aging curve obtained after treatment at 420 ℃ for 24 h and subsequent aging at 150 ℃ reflects the typical influence of the aging process. The hardness for aging at 150 ℃ increases gradually and does not reach the peak value in the time range considered(24 h). However, ageing at 380 ℃ results in a rapid increase of hardness in 6 h, reaching a peak at about 10 h. The hardness remains at the maximum value for a significant period in the time range considered. From these results, it is concluded that the ageing at 380 ℃ accelerates atomic diffusion and decomposition of the supersaturated solid solution.

The electrical resistivities of AZ91 alloy by aging treatment at 150 ℃ and solid solution treatment at 420 ℃ are plotted as a function of time in Figs. 4(a) and (b), respectively. For solid treatment at 420 ℃, the first point(0 h) of the electrical resistivity curve corresponds to the value of the as-cast AZ91 alloy via LFC. The electrical resistivity increases with time from 0 to 18 h before reaching at the maximum value. The electrical resistivity does not show a notable variation at the end of solid treatment, which means that the most of the precipitates have dissolved into the matrix. The electrical resistivity curve decreases at the start of aging at 150 ℃, followed by an increase to the peak value, and subsequently the curve starts to decrease.

In this experiment, the supersaturated solid solution of alloy was obtained by quenching specimens to room temperature. The vacancies in the solution-treated specimen for 24 h were "quenched-

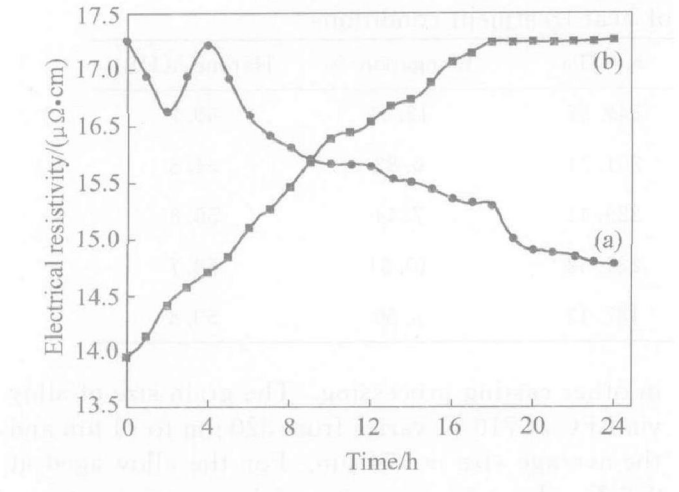

Fig. 4 Electrical resistivity curves for AZ91
(a) —Aged at 150 ℃; (b) —Solution-treated 420 ℃

in"[19]. During aging the β phase precipitate out from the matrix in two forms: discontinuous and continuous precipitation[20]. Both vacancies and precipitates make significant contributions to the electrical resistivity. In the first range(0 – 2 h) of aging at 150 ℃, the slight decrease of resistivity might be due to a sort of rearrangement and annihilation of quenched-in vacancies. The reasons of the observed resistivity rise in the second range(2 – 4 h) of aging might be attributed to the formation and growth of small solute atoms clusters in pre-precipitation stage. A critical size of the clusters, comparable with the wavelength associated with the electrons, would cause the greatest disturbance to conduction electron flow. In the third range(4 – 24 h) of aging at 150 ℃, the decrease in resistivity might be due to the decrease of the scattering power of precipitates as their size increases in the matrix.

3.3 Mechanical properties

The grain size and mechanical properties of as-cast AZ91 alloy under different conditions are compared in Table 3. With the decrease of casting temperature from 740 to 680 ℃, the ultimate tensile strength, yield strength, hardness and elongation of the alloy via LFC increase slightly whereas the grain size decreases. In the case of the same casting temperature, the values of tensile properties and hardness under permanent mould casting are much higher than those of alloy via LFC. Obviously, the improvements in tensile strength and hardness can be mainly ascribed to fine-grain strengthening due to grain-boundaries blocking dislocations. It is noticeable that the mechanical properties of AZ91 cast via LFC are superior to those of sand-cast alloy. Compared to the empty-cavity sand mould, the molten AZ91 alloy filling behavior in the lost foam mold is much more complex. Since polymer degradation is highly endothermic, this degradation produces a chilling effect that can result in a high degree of undercooling in the liquid metal[11, 20]. In addition, the cushioning effect due to the presence of foam patterns can alleviate or eliminate entrapment of gas during the metal filling process. Obviously, the two factors both have a beneficial effect in improving the mechanical properties.

Tensile properties and hardness of AZ91 alloys in five different heat treatment conditions are shown in Table 4. It can be seen from the table that the hardness, tensile strength and yield strength of the alloy are significantly improved after heat treatment. However, the yield strength is the lowest in the case of solution-treated material that makes the solute-treated alloy unsuitable for some applications. A tendency of an increase in the tensile strength, yield strength, hardness and elongation with aging time at 150 ℃ is observed. This can be attributed to the increase of number of the precipitates per unit volume[21]. Compared to alloy aged at 380 ℃ for 8 h, the alloy aged at 380 ℃ for 24 h shows a drop in tensile properties and hardness due to the coarse second phases that make them inefficient obstacles to dislocation movement. Aging carried out at higher temperature leads to a greater completeness of diffusion. As a result, alloy aged at 380 ℃ for 8 h has higher ultimate tensile strength, yield strength, elongation and hardness than alloy aged at 150 ℃ for 8 h. The table shows that aging at high temperature is more effective for improving tensile strength and yield strength.

Table 3 Grain size and room-temperature mechanical properties of as-cast AZ91 alloy under different processings

Processing(Casting temperature)	Grain size/μm	$\sigma_{0.2}$/MPa	σ_b/MPa	Elongation/%	Hardness(HB)
Lost foam casting(680 ℃)	172	102.69	158.04	2.50	54.5
Lost foam casting(740 ℃)	177	94.78	155.89	2.25	53.8
Lost foam casting(710 ℃)	174	101.49	156.43	2.36	54.5
Resin bonded sand gravity casting(710 ℃)	183	95.44	150.43	2.19	52.8
Permanent mould casting(710 ℃)	107	105.33	168.69	2.52	70.6

Table 4 Room-temperature mechanical properties of AZ91 alloy via lost foam casting after a series of heat-treatment conditions

Heat-treatment	$\sigma_{0.2}$/MPa	σ_b/MPa	Elongation/%	Hardness(HB)
Solution-treated for 24 h	84.57	249.92	13.61	50.7
Aging for 8 h at 150 ℃	102.50	201.71	6.83	54.3
Aging for 24 h at 150 ℃	105.11	229.41	7.44	56.8
Aging for 8 h at 380 ℃	105.49	231.52	10.61	58.7
Aging for 24 h at 380 ℃	93.37	187.12	5.50	59.8

The effect of heat treatment on the flow behavior is better appreciated in the flow curves of Fig. 5. These curves have been plotted as true stress versus true plastic strain to emphasis the changes in the work-hardening rate in the true plastic strain ranges. Yielding is very gradual and departure from linear elastic deformation occurs at a very low stress. It can be seen that the work-hardening rate of the solid-treated alloy is the lowest of all the samples. However, the highest plastic strain is observed in the solid-treated alloy. Compared to the as-cast alloy, aging causes an increased work-hardening rate. The alloy aged at 380 ℃ for 8 h and the alloy aged at 150 ℃ for 24 h exhibit nearly the same work-hardening rate at low strain. From the results, it can be concluded that aging, especially high-temperature aging, is quite beneficial in improving the work-hardening rate of plastic deformation.

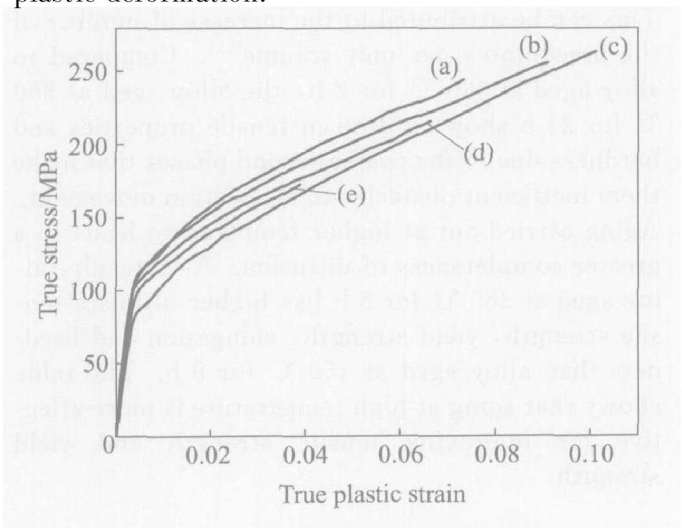

Fig. 5 Flow curves of AZ91 alloys
(a) —Aged for 24 h at 150 ℃; (b) —Aged for 8 h at 380 ℃; (c) —Solid-treated for 24 h at 420 ℃; (d) —Aged for 8 h at 150 ℃; (e) —As-cast

4 CONCLUSIONS

1) The microstructure of the AZ91 alloy via LFC consists of dominant α-Mg and β-$Mg_{17}Al_{12}$ as well as a new phase $Al_{32}Mn_{25}$ with size of about 5 - 50 μm, which has not been detected in AZ91 alloy in other casting processing. The grain size of alloy via LFC at 710 ℃ varies from 320 μm to 41 μm and the average size is 174 μm. For the alloy aged at 380 ℃, the precipitates appear in a continuous pattern at grain boundaries and in the grains. However, when aging for 24 h at 150 ℃, the discontinuous precipitates emerge at grain boundaries and have a massive form.

2) From the solution and aging curves of AZ91 alloy via LFC, it is concluded that the prolonged exposure of the aged specimen at 380 ℃ accelerates atomic diffusion and decomposition of the supersaturated solid solution. The variation of electrical resistivity in isothermal aging process reflects the combination effects of the "quenched-in" vacancies and precipitates.

3) In the case of same casting temperatures, the mechanical properties of AZ91 alloy via LFC are superior to those of sand-cast alloy due to chilling effect and cushioning effect. The hardness, elongation to fraction and tensile strength of the alloys are significantly improved after heat treatment. Aging at high temperature is more effective for improving tensile strength and yield strength and the work-hardening rate of plastic deformation.

REFERENCES

[1] Brungs D. Light weight design with light metal casting [J]. Materials & Design, 1997, 18(4/6): 285 - 291.
[2] Cole G S. Issues that influence magnesium's use in the automotive industry [J]. Materials Science Forum, 2003, 419 - 422(1): 43 - 50.
[3] Kaneko T, Suzuki M. Automotive applications of magnesium alloys [J]. Materials Science Forum, 2003, 419 - 422(1): 67 - 72.
[4] Mordike B L, Ebert T. Magnesium properties —application —potential [J]. Materials Science & Engineering, 2001, A302(1): 37 - 45.
[5] Lee S, Lee S H, Kim D H. Effect of Y, Sr and Nd additions on the microstructure and microfracture mechanism of squeeze-cast AZ91-X magnesium alloys [J]. Metallurgical & Materials Transactions, 1998, 29A(4): 1221 - 1235.
[6] Kleiner S, Beffort O, Wahlen A, et al. Microstructures and mechanical properties of squeeze cast and

semi-solid cast Mg-Al alloys [J]. Journal of Light Metals, 2002, 2(4): 277-280.
[7] Sanchez C, Nussbaum G, Azavant P, et al. Elevated temperature behavior of rapidly solidified magnesium alloys containing rare earths [J]. Materials Science & Engineering, 1996, A221(1/2): 48-57.
[8] Dahle A K, Lee Y C, Nave M D, et al. Development of the as-cast microstructure in magnesium-aluminum alloys [J]. Journal of Light Metals, 2001, 1(1): 61-72.
[9] Dahle A K, Sannes S, St. John D H, et al. Formation of defects bands in high pressure die cast magnesium alloys [J]. Journal of Light Metals, 2001, 1(2): 99-103.
[10] Ajdar R, Ravindran C, Mcclean A. Total solidification time and flow length of A356 alloy during lost foam casting [J]. Transactions of the American Foundry Society, 2002, 110(147): 1497-1513.
[11] Shivkumar S. Casting characteristics of aluminum alloys in the EPC process [J]. Transactions of the American Foundry Society, 1993, 101(152): 513-518.
[12] Zhao Q, Burke J T, Gustafson T W. Foam removal mechanism in aluminum lost foam casting [J]. Transactions of the American Foundry Society, 2002, 110(83): 1399-1414.
[13] Wang C, Ramsay C W, Askeland D R. Processing variable significance on filling thin plates in the LFC process—the staggered, nested factorial experiment [J]. Transactions of the American Foundry Society, 1997, 105(138): 427-434.
[14] Liu J, Ramsay C W, Askeland D R. Effects of foam density and density gradients on metal fill in the LFC process [J]. Transactions of the American Foundry Society, 1997, 105(139): 435-442.
[15] Hirt C W, Barkhudarov M R. Predicting defects in lost foam castings [J]. Modern Castings, 2002, 92(12): 31-33.
[16] Liu Z L, Hu J Y, Wang Q D, et al. Evaluation of the effect of vacuum on mold filling in the magnesium EPC process [J]. Journal of Materials Processing Technology, 2002, 120(1-3): 94-100.
[17] Bag A, Zhou W. Tensile and fatigue behavior of AZ91D magnesium alloy [J]. Journal of Materials Science Letter, 2001, 20(5): 457-459.
[18] Ambat R, Aung N N, Zhou W. Studies on the influence of chloride ion and PH on the corrosion and electrochemical behavior of AZ91D magnesium alloy [J]. Journal of Applied Electrochemistry, 2000, 30(7): 865-874.
[19] Haasen P. Mordike J Tr. Physikalische Metallkunde [M]. London: Cambridge University Press, 1978.
[20] Pan E N, Sheu G L. Mold filling behavior in vertical gating lost foam aluminum alloy [J]. Transactions of the American Foundry Society, 2001, 109(79): 1503-1521.
[21] Celotto S. TEM study of continuous precipitation in Mg-9wt%Al-1wt%Zn alloy [J]. Acta Materialia, 2000, 48(8): 1775-1787.

(Edited by YANG Bing)